crystals

Review

Surface Dispersion Suppression in High-Frequency GaN Devices

Pengfei Zhu, Xianfeng Ni, Qian Fan and Xing Gu *

Institute of Next Generation Semiconductor Materials, Southeast University, Suzhou 215123, China
* Correspondence: xinggu@seu.edu.cn

Abstract: GaN-based high electron mobility transistors (HEMTs) are shown to have excellent properties, showing themselves to perform well among the throng of solid-state power amplifiers. They are particularly promising candidates for next-generation mobile communication applications due to their high power density, frequency, and efficiency. However, the radio-frequency (RF) dispersion aroused by a high surface-state density inherent in nitrides causes the degradation of GaN devices' performance and reliability. Although various dispersion suppression strategies have been proposed successively—including surface treatment, passivation, field plate, cap layer, and Si surface doping—outcomes were not satisfactory for devices with higher frequencies until the emergence of a novel N-polar deep recess (NPDR) structure broke this deadlock. This paper summarizes the generation of dispersion, several widespread dispersion containment approaches, and their bottlenecks under high frequencies. Subsequently, we highlight the NPDR structure as a potential substitute, evaluate its technical benefits, and review the continuous exertions in recent years.

Keywords: GaN-based HEMTs; RF dispersion; suppression; NPDR structure; high-frequency

check for updates

Citation: Zhu, P.; Ni, X.; Fan, Q.; Gu, X. Surface Dispersion Suppression in High-Frequency GaN Devices. *Crystals* **2022**, *12*, 1461. https://doi.org/10.3390/cryst12101461

Academic Editor: Dmitri Donetski

Received: 27 September 2022
Accepted: 14 October 2022
Published: 16 October 2022

1. Introduction

Millimeter-wave technology is undoubtedly an ongoing research focus for fifth-generation mobile communication technology (5G) and beyond. GaN-based high electron mobility transistors (HEMTs) are taking the lead in the radio-frequency (RF) industry, especially for those applications that require abundant power density, thanks to the unparallel combined material properties of a wide bandgap (E_g ~ 3.4 eV), large critical breakdown electric field, high electron saturation velocity, high electron mobility and sheet density achieved by 2-Dimensional electron gas (2DEG), and excellent thermal properties when prepared on silicon carbide (SiC) substrates [1–4]. However, the existence of direct current (DC)-RF dispersion (also known as the "current collapse") leads to a significant decrease in output power density and causes reliability-related issues in GaN-based HEMTs, especially at higher frequencies, which limits the development and application of such devices. Research has shown that the widespread presence of trapping states (covering the semiconductor surface, barrier layer, interface, channel, and buffer layer) in III/V group compound semiconductors should be mainly responsible for the dispersion of GaN HEMTs [5]. In high-frequency devices, the closer proximity of 2DEG to the surface highlights the role of surface traps (surface states) on dispersion [6,7]. These surface states trapping electrons to form a "virtual gate" (similar to a gate function) further deplete the 2DEG channel, which strongly impacts the device output characteristics and reliability. Engineers have tried to solve this problem by using multiple processes, including surface treatment [8], passivation [9], field plate [10], cap layer [11], and Si surface doping [12] in recent years. With the increasing demand for higher operating frequencies, the reduced gate length and the aspect ratio in need of being maintained drive the 2DEG much closer to the surface compared with the lower frequency HEMT epitaxial structure, thus limiting the effectiveness of those techniques in improving the dispersion. In this vein, researchers working on high-frequency GaN devices have sought novel technologies to better solve this aporia.

In this paper, we explain the origin of surface states and the mechanism causing dispersion in GaN devices. The current dominant methods for suppression dispersion and their bottlenecks in the high-frequency domain are summarized. Finally, we focus on the N-polar deep recess (NPDR) structure, addressing its uniqueness in controlling dispersion and reviewing the research advances in NPDR metal-oxide-semiconductor (MIS)-HEMTs.

2. Surface States and Virtual Gate

In GaN-based HEMTs, surface states are critical sources of 2DEG in the channel [13], allowing the device to achieve a very high electron concentration without the need for intentional doping (unlike GaAs-based 2DEG), which dramatically reduces ionized impurity scattering and enhances carrier mobility. On the other hand, GaN-based HEMTs are also plagued by the dispersion effect generated by surface states. This section mainly discusses the creation of surface states and the principle of dispersion caused by them.

2.1. Sources of Surface States

Surface states, a type of electron-bound state, can be categorized into two sorts based on their formation: intrinsic and extrinsic.

Intrinsic surface states arise due to the termination of the ideal crystal structure at the surface. It is common knowledge that GaN, like any crystal, cannot be extended infinitely in space. Therefore, the periodic potential field will be interrupted at the surface and cause additional energy levels in the forbidden band known as surface energy levels, whose corresponding electronic states are named surface states. Chemical bonding theory explains that the chemical bonds of GaN crystal break at the surface, and the unbonded electron pairs form dangling bonds, the corresponding electronic states being surface states [14]. Besides, those created by threading dislocations accessible at the surface, native oxide, N-vacancies, ions adsorbed from the surrounding environment (such as oxygen, carbon, and hydrogen, each with its unique energy level), and surface damage in the processing are referred to as extrinsic surface states [14–16]. These two different forms of generation pathways are shown in Figure 1.

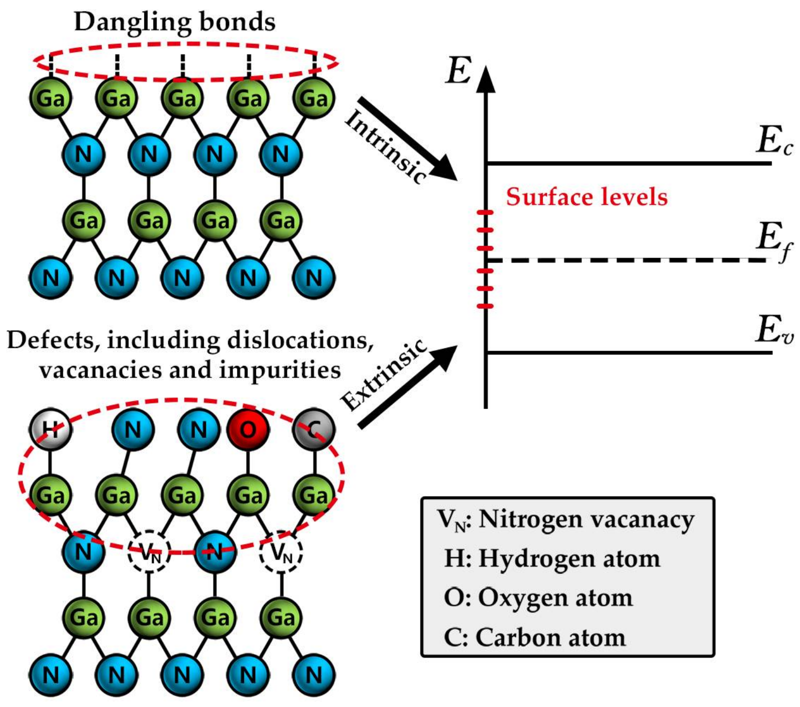

Figure 1. Mechanisms for the generation of intrinsic and extrinsic surface states.

2.2. Virtual Gate Model

Depending on their behaviors, surface states can be classified as either acceptors or donors. Table 1 shows the charge situations of these two categories of surface states in the empty and filled (after trapping the electrons) conditions. Under the strong influence of the polarized electric field, the donor surface state filled with electrons below the Fermi level will be partly ionized, allowing the electrons to escape into the channel to produce a high concentration of 2DEG and leave large positive charges on the surface [17]. As such, the surface of the GaN device should not show a negative surface potential. Vetury et al. [18] observed that a significant number of negative charges reside on the device's surface, conflicting with the previous theory when they employed the floating gate approach to investigate the surface state impact of AlGaN/GaN HEMTs in 2001. In response, they explained that these positive charge centers (empty surface states) located between the gate and drain act like traps to capture gate leakage electrons or those channel hot electrons escaping via the barrier to the surface [15,19,20]. During the process from off-state to on-state, electron emission from surface states with a slower period differs from RF signals, so the trapped electrons are not released when the device is turned on, which is equivalent to another gate existing between the gate and the drain electrodes, i.e., virtual gate [21,22]. As shown in Figure 2, the trapped electrons move and jump on the surface to form a negative charge region, causing the gate depletion region to expand laterally, depleting the 2DEG in the channel and resulting in the current collapse. This RF dispersion is generally determined by pulsed I_{DS}–V_{DS} measurement, depending on different stressed conditions, and can be defined as:

$$\text{Dispersion } (\%) = \frac{I_{DS,DC} - I_{DS,Pulsed}}{I_{DS,DC}} \times 100\% \tag{1}$$

Table 1. Electrical properties of donor and acceptor surface states.

Type	Empty	Filled
Donor surface states	Positive	Neutral
Acceptor surface states	Neutral	Negative

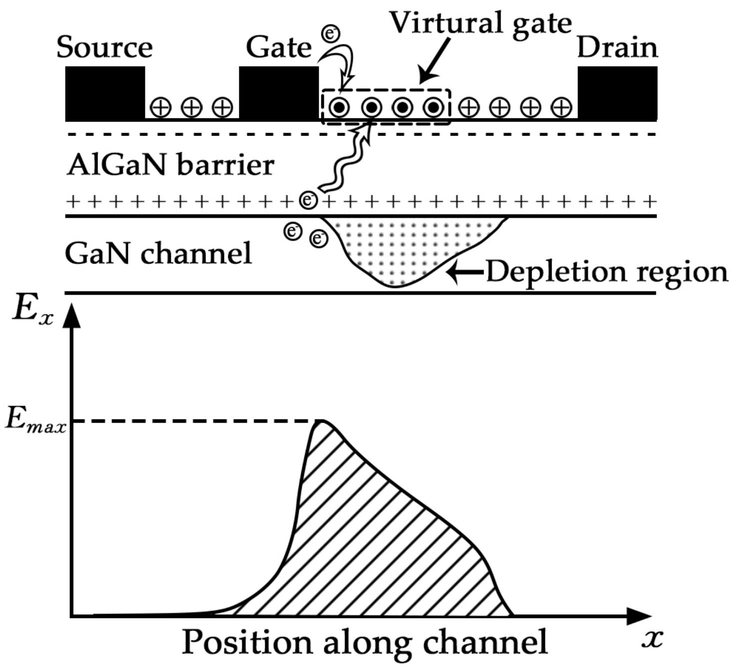

Figure 2. The device model shows the virtual gate's location, schematic representation, and the electric field distribution in the channel.

3. Methods for Suppression Surface Dispersion and Their Bottlenecks

Based on the principle of extra depletion of the 2DEG channel by the virtual gate model, it can be concluded that one of the most critical tasks in dispersion control is to minimize trapping electron action attributable to surface states. Common solutions in AlGaN/GaN HEMTs are summarized in Figure 3. Five categories of methods have been developed and demonstrated to suppress the RF dispersion with mixed success: (1) surface treatment that intends to diminish surface state density to reduce the odds of surface states trapping electrons; (2) passivation, which intends to bury surface traps by depositing dielectrics on the device surface to prevent gate leakage electrons from being trapped in them; (3) the uses of field plate structure intend to alleviate the gate edge electric field crowding and enhance the emission rate of trapped electrons; (4) adding a GaN cap intends to control the gate-lag caused by the leakage current; (5) si surface doping intends to compensate for the trapping energy level to screen the 2DEG from the traps. This section summarizes the research advances of the above technologies and the bottlenecks they encounter at high frequencies.

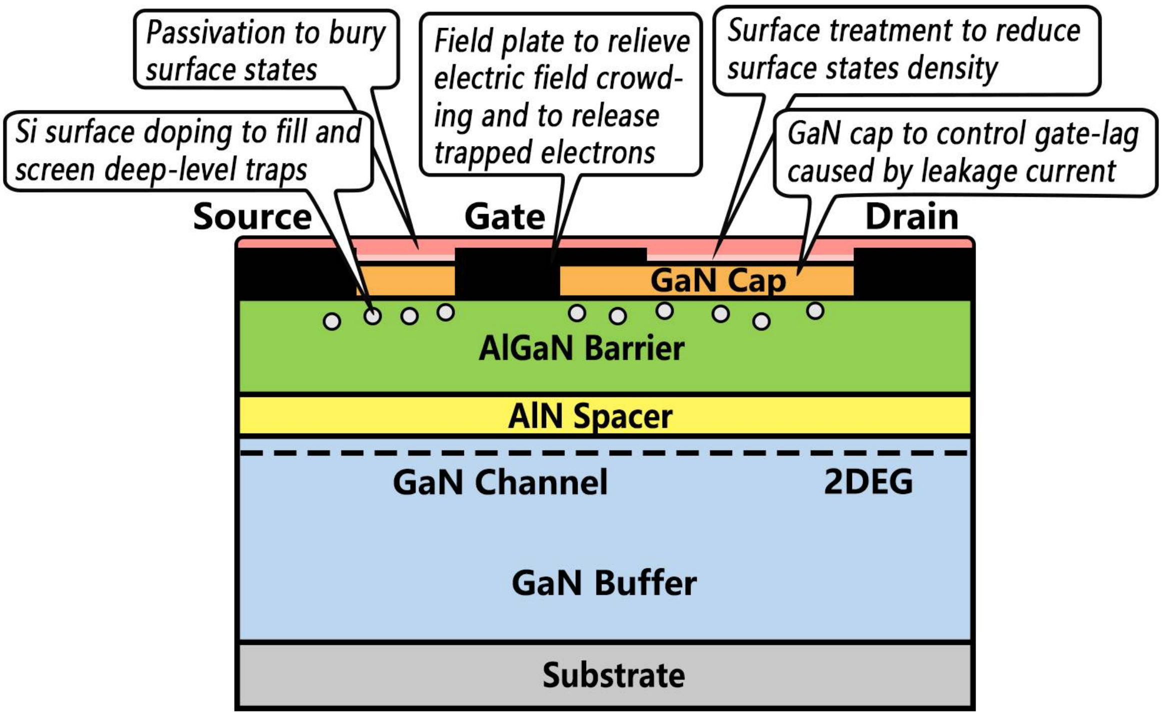

Figure 3. Common methods for suppressing RF dispersion in AlGaN/GaN HEMTs.

3.1. Common Methods for Suppression Surface Dispersion

3.1.1. Surface Treatment

Natural oxides and organic matter adsorbed on the (Al)GaN surface create many interface states between the dielectric used for passivation and the barrier, which reduces the effectiveness of passivation. Consequently, surface treatment prior to dielectric deposition is of extraordinary importance to obtain a high-quality interface.

Organic matter and oxides are mainly composed of carbon and oxygen. UV/ozone surface treatment can proficiently remove carbon [23], while oxygen can be treated by some wet chemical cleaning methods. King et al. [24] found that HF and HCl were able to minimize oxygen coverage on AlN and GaN surfaces, and residual halogen ions (cl^- and F^-) tie up the dangling bonds preventing the surface from being oxidized again. The same result was found in the experiments of Diale et al. [25], who respectively compared the methods of cleaning GaN surfaces with HCl, KOH, and $(NH_4)_2S$. They concluded that KOH was effective for carbon removal but contributed to a rough surface. The sample cleaned in $(NH_4)_2S$, a chemical avoiding surface re-oxidation, acquired the optimum cleaning result with the lowest values of both C and O, root mean square (RMS) roughness, and Ga/N ratio. Other wet chemical cleaning efforts mainly focus on HNO_3, H_2SO_4, NH_4OH, and NaOH.

Surface treatment using plasma like NH_3, N_2, and N_2O is also valuable for suppressing dispersion to enhance performance [26–29]. By filling nitrogen vacancies and removing impurity oxygen atoms, nitrogen-related plasma treatment considerably enhances the quality of the SiN_x/GaN interface [28]. Romero et al. [27] treated the AlGaN/GaN HEMT (which had been wet cleaned by NH_4OH) with in situ N_2 plasma (N_2PP) at 200 °C for 1 min prior to SiN_x passivation of the device. The treated GaN HEMT obtained an $I_{DS,}$ which was 10% higher than the untreated one, and achieved a more advanced knee voltage. A 65% drop in the density of interface states was discovered after applying N_2PP, which was responsible for reducing gate leakage current by two to three times (from 7.7 to 2.3 × 10^{-2} A/cm^2 at $V_{GD} = -20$ V), utilizing capacitance-voltage (C–V) and conductance-frequency (G-F) measurements. Furthermore, NH_3 plasma-treated performs better than N_2 in GaN HEMTs [26], with RF dispersion respectively decreasing from 63% (without pretreatment) to 1% and 9% (shown in Figure 4). This is probably due to the fact that NH_3 plasma eliminates oxide and carbon residues while reducing the density of surface state defects.

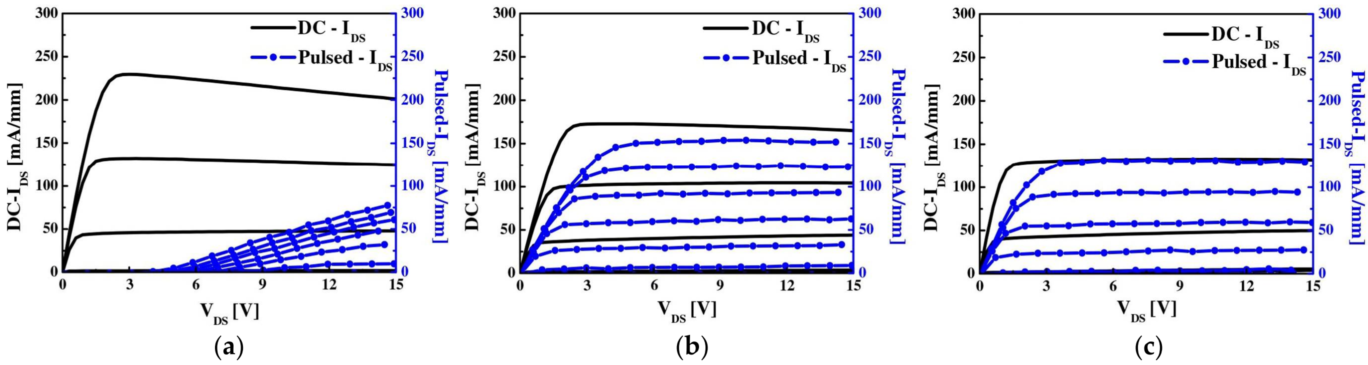

Figure 4. DC and pulsed I_{DS}–V_{DS} characteristics for the GaN device. (**a**) Without pretreatment; (**b**) with NH_4OH/N_2 pretreatment; (**c**) with NH_4OH/NH_3 pretreatment. DC and pulsed I_{DS}–V_{DS} were measured at V_{DS} = 0 to 15 V and $V_{GS} = -3$ to 1 V. The pulse width and period were 500 ns and 1 ms. Adapted with permission from Ref. [26]. Copyright 2010, The Japan Society of Applied Physics.

In addition, plasma can also be combined with heat treatments such as high-temperature annealing in vacuum [30] or N_2 [31] and NH_3 [32] atmospheres to enhance the desorption of contaminants further and assist in the elimination of remaining surface defects, thereby improving the surface quality of the device. It has to be emphasized, however, that the surface treatment also increases the risk of unreliability and is, therefore, mostly involved in laboratory research efforts.

3.1.2. Passivation

Since 2000, when Green et al. [15] deposited a layer of Si_3N_4 for passivation on the surface of AlGaN/GaN HEMT to obtain the highest power density (4 W/mm at 4 GHz) during that period, passivation has become one of the most commonly used and effective techniques to solve RF dispersion after more than 20 years of development.

Previous studies have reported that SiN_x, AlN, SiO_2, SiNO, Al_2O_3, and HfO_2 (high-κ dielectric) can all be applied to GaN-based HEMTs [28,31,33–35]. However, some researchers believe that nitrides (compared to oxides) probably are more suitable for GaN devices because oxygen impurities can easily diffuse into the GaN crystal and generate a high density of deep (or slow) interface states, producing additional current collapse [36,37]. This conclusion is consistent with the report of Geng et al. [31], which evaluated AlGaN/GaN MIS-HEMTs utilizing PECVD deposition of 20 nm SiN_x, SiO_2, and SiNO as passivation layers, respectively. It is found that the interface-trapped charge density (or the deep energy level defects density with long emission time of electrons) for $\Delta E > 0.657$ eV in SiO_2 is 4.13 × 10^{12} cm^{-2} (three times larger than that of SiN_x, ~1.38 × 10^{12} cm^{-2} in SiN_x). Compared to only 11.06% dispersion in SiN_x, the current collapse in SiO_2 reaches 84.14% at $V_{gs} = -18$ V, proving the success of SiN_x passivation and the fact that SiO_2 would not be appropriate for GaN devices. Based on taking SiN_x as a dielectric, Huang et al. [38] proposed an improved structure using bilayer LPCVD SiN_x; a Si-rich SiN_x layer (Si/N = 59/41) with a thickness of ~10 nm was first deposited, followed by a ~67 nm Si-poor SiN_x layer (Si/N = 50/50, high-resistive). Figure 5 exhibits a TEM cross-sectional image of this bilayer SiN_x passivation, and the black dotted line refers to the boundary between the first and second layers. The Si-rich SiN_x layer upper to surface is argued to remove the deep-level traps at the AlGaN/SiN_x interface, which makes microwave GaN HEMTs show a much smaller degradation of about 9.7% (~30% dispersion in 70 nm Si-poor SiN_x sample) while maintaining a low gate leakage current owing to the second high-resistive layer.

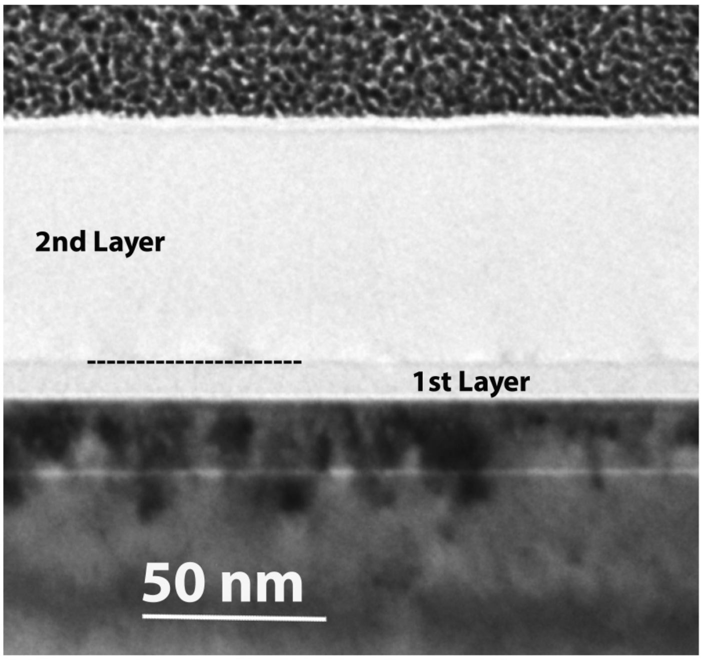

Figure 5. TEM cross-sectional image shows a distinguishable bilayer structure of the passivation layer. Reprinted with permission from Ref. [38]. Copyright 2018 by IEEE.

3.1.3. Field Plate

The field plate is applied in GaN-based HEMTs to reduce the electric field crowding at the gate corner of the drain side, preventing electron injection from the gate into surface states, and forming a virtual gate. Moreover, the horizontal electric field near the end of the field plate will strengthen the process of electrons escaping from the traps and speed up the electrons hopping along the AlGaN surface, further lowering the trapped electron density and, therefore, substantially suppressing current collapse [22]. The effectiveness of the field plate in suppressing current collapse is more robust with increasing field plate length. The trapped charges on the device surface decreased from 1.58 × 10^{12} cm^{-2} (no field plate) to 0.8 × 10^{12} cm^{-2} after using a 1.5 μm field plate structure [39], the pulsed I_{DS}–V_{DS} characteristics and trapped charge density are displayed in Figure 6. The field plate this method has now been widely adopted and greatly influenced the high-voltage devices. Despite this, it is worth noting that it is thrown into an awkward situation in high-frequency applications. Because this design not only reduces the speed of the channel electrons owing to the weakened electric field but also introduces additional external capacitance that limits the efficiency and gain of the device. Accordingly, in order to ensure anticipant RF performance, the field plate has found very limited usage in high-frequency industries.

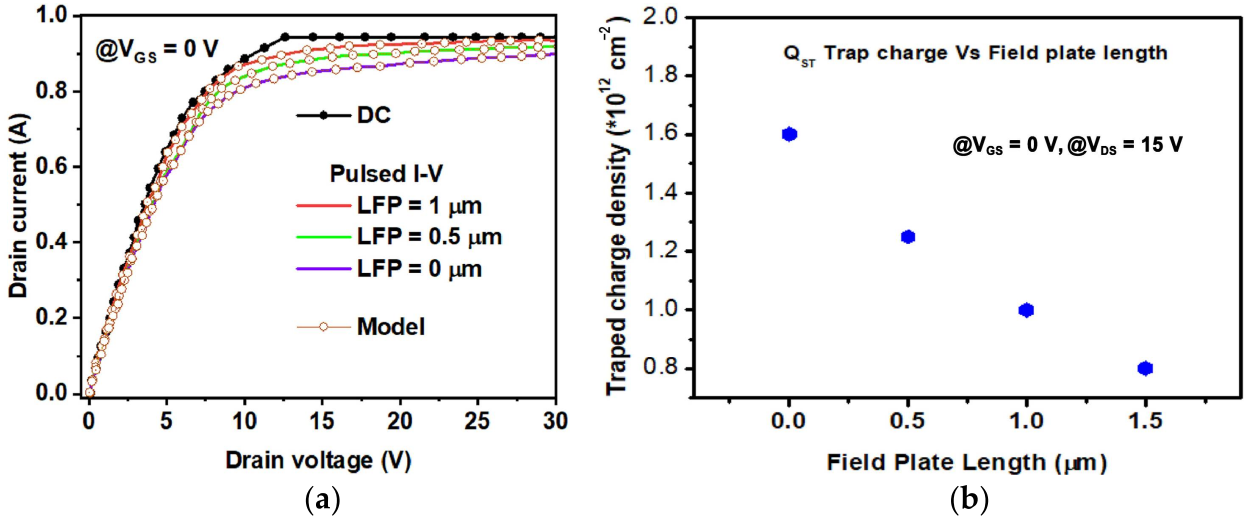

Figure 6. AlGaN/GaN HEMT characteristics with different field plate lengths. (**a**) Pulsed I_{DS}-V_{DS} characteristics with Quiescent Voltage ($V_{GS,Q}$ = −8 V and $V_{DS,Q}$ = 50 V); (**b**) trapped charge (Q_{ST}). Adapted with permission from Ref. [39]. Copyright 2021 by Elsevier.

3.1.4. GaN Cap

GaN cap, a thin layer of GaN (about a few nanometers) on top of the barrier that forms a sandwich structure (e.g., GaN/AlGaN/GaN), is another well-established technique in industry for managing the current collapse. This cap can be doped GaN (typically n-type doping by SiH_4 or p-type doping by Cp_2Mg) or i-GaN. No matter what type of GaN cap is used, it degrades gate leakage levels [40], both vertically and horizontally. Vertically, raising the effective Schottky barrier by the GaN cap provides a stronger limitation on the emission and tunneling of hot electrons [11,41]. Horizontally, as presented by Sarkar et al. [11], the GaN cap passivates the access region to suppress lateral electrons hopping via surface traps, significantly reducing the total leakage current (shown in Figure 7a). In other words, the GaN cap can effectively screen 2DEG from dispersion-related traps. As shown in Figure 7b,c, 2 nm of GaN cap layer effectively controls the current collapse in GaN-based HEMTs, while enhancing the device's frequency performance (62% improving in f_T) at the expense of a small amount of gain.

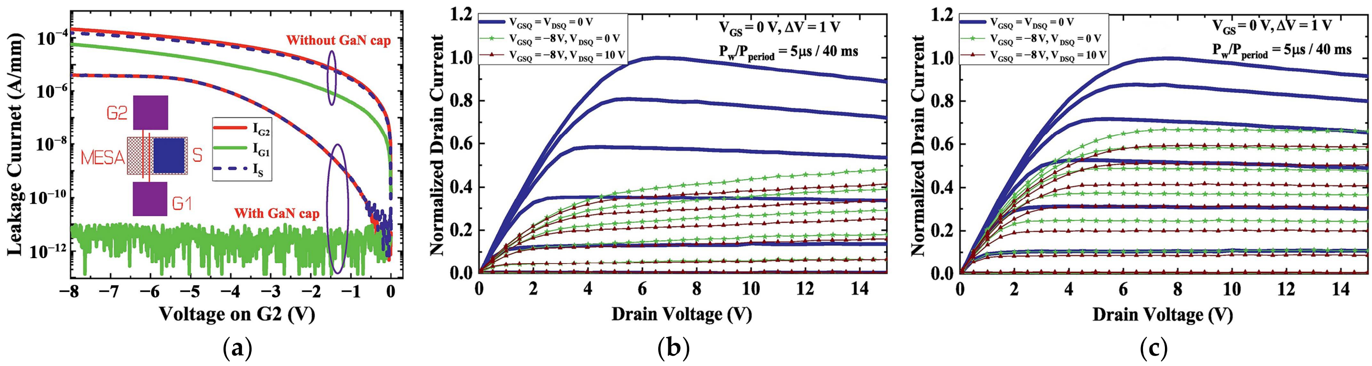

Figure 7. (**a**) Characteristics of the double gate. I_s is the vertical leakage current through 2DEG, and I_{G1} is the horizontal leakage current by electron hopping between surface states. I_{G2} is the total leakage current (I_{G2} = I_S + I_{G1}). Pulsed output characteristics of HEMTs, (**b**) without GaN cap, and (**c**) with GaN cap. Adapted with permission from Ref. [11]. Copyright 2022 by Elsevier.

3.1.5. Si Surface Doping

Surface doping of GaN HEMTs with Si also contributes to the suppression of dispersion [42]. Si (as an electron donor) surface doping can prevent the slow process of re-emitting trapped channel electrons from surface states by filling and screening the deep-level traps [12]. However, the method also causes an escalation in leakage levels (electrons can tunnel through the thinned potential barriers more easily), so attention to a concentration should be paid when doping the surface of the device to avoid the impact of poor leakage current and breakdown resistance on device reliability.

3.2. Bottlenecks Encountered at High Frequencies

At lower frequencies (below Ka-band), the previously mentioned techniques can be combined to control RF dispersion in GaN HEMTs. As the gate length is further decreased to increase the operating frequency, the distance from the polarized surface to the 2DEG channel also has to be reduced to maintain the desired aspect ratio and contain the short channel effect, whereas the corresponding cost is the 2DEG channel suffers from the surface RF dispersion more seriously, rendering the effect of all surface engineering techniques less effective. When the operating frequency is pushed over 30 GHz (which means just entering the millimeter-wave range), the capacitance penalty imposed by the field plate causes this structure to be disabled because of the severely degraded high-frequency performance. Therefore, researchers urgently need to find new techniques to alleviate the problem of surface state trapping electrons to ensure the device's reliability at high-frequency operation.

4. NPDR MIS-HEMTs for High-Frequency Device

Due to the comparatively good material quality and electrical features, Ga-polar GaN has dominated power devices for a long time. In recent years, the material growth technique has constantly been progressing on N-polar GaN; thus, related device research gradually gained significant interest [43,44]. On account of the opposing polarity, N-polar GaN HEMTs offer a series of natural advantages for higher frequency epitaxy and device design over the Ga-polar [45], such as (a) devices with a narrower top layer bandgap achieve lower contact resistance; (b) a natural back-barrier improves 2DEG confinement and minimize short channel effect while giving rise to higher transconductance. Additionally, the presence of the back-barrier allows the device to keep leakage current (from channel to substrate) at a low range even when there is no doping (e.g., Fe, C) in the buffer, avoiding the dispersion introduced by slow deep energy level discharge [46]; (c) flexible device aspect ratios accommodate shorter gate lengths resulting from increased frequency. These features are tailored to the needs of high-frequency devices so that the N-polar GaN transistor stood distinctly above all others in 2012, with a f_T = 270 GHz and f_{max} = 370 GHz [47]. However, the most outstanding value of N-polar GaN materials is the ability to make the deep recess structure dramatically mitigate RF dispersion to guarantee reliability at higher frequencies [48]. Here, the basic structure of NPDR is displayed, the reason why deep recess can only be applied on the N-polar GaN (rather than Ga-polar) is discussed, and the research advances on NPDR are summarized.

4.1. What and Why Is NPDR?

The most basic structure of NPDR is to directly thicken the GaN channel above the back-barrier, as shown in Figure 8a, and the 2DEG at the bottom of the channel is isolated from the surface to control dispersion. The gate is buried deep in the GaN channel to considerably boost vertical scaling and strengthen the gate's modulation of 2DEG. To avoid gate leakage currents and regulate the dispersion created by the sidewall, a thin layer of dielectric (normally MOCVD SiN_x) is commonly placed for initial passivation before depositing gate metal. In the improved design of the NPDR structure (shown in Figure 8b), the insertion of an AlGaN cap layer (as etch stop layer) is considered necessary because the difference in components allows for more precise selective etching, while the cap provides better Schottky contact for the device. Apart from these two causes, the polarization electric field generated by N-polar AlGaN also mitigates the injection of gate leakage electrons during reverse bias [49]. Since the thick GaN cap keeps the surface away from the channel (differs from passivation, thick dielectric does not change the surface position due to the absence of polarization), even if a virtual gate is formed on the surface of the access region, there is almost no depletion of charge in the channel. The scattering associated with the surface is also effectively controlled, thus substantially increasing the 2DEG mobility. As mentioned earlier, the traditional passivation of HEMTs using ex situ SiN_x dielectrics still has massive trapping states, whether in bulk or at the interface. However, no significant interfacial states are presented in the NPDR structure because the GaN cap has no difference in lattice constants from the channel. There should also be no more bulk traps within the UID GaN cap than in the channel, which ensures an ultra-low trap density near the 2DEG. To sum up, the deep recess structure is impressive for eliminating the RF dispersion in GaN HEMTs.

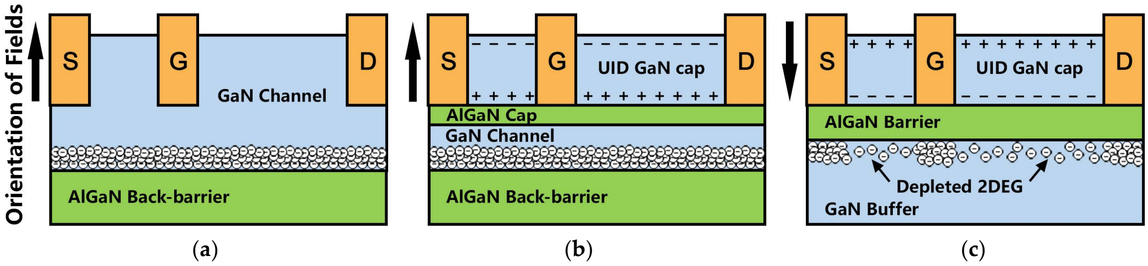

Figure 8. Schematic diagrams of on-state device operation for deep recess GaN HEMT with different structures. (**a**) N-polar; (**b**) N-polar with AlGaN cap; (**c**) Ga-polar.

In fact, deep recess structures were first proposed for Ga-polar devices [50–52], but the results did not meet the expectations. As the polarization of the GaN cap caused the conduction band to be pulled up, the 2DEG would be depleted below the access region (shown in Figure 8c). Shen et al. speculated that suitable Si doping could compensate for the negative polarization charge and prevent the accumulation of holes. They proposed direct Si delta-doping at the GaN/AlGaN interface [52], but unfortunately, the introduction of Si would cause higher gate leakage and, thus, a reduction in breakdown voltage. Another method that insets a Si-doped graded AlGaN between the UID GaN cap and the AlGaN barrier is introduced for similar motivations [50]. Although the lower Al component of AlGaN can partially alleviate the 2DEG depletion by polarization, it is difficult to overcome the process because of the high requirements for precise etching. The additional graded AlGaN is also detrimental to the device aspect ratio. Hence, it can be confirmed that using a deep recess structure on the Ga-polar must be compromised for device performance.

In contrast to the Ga polarity, the electric field created in the access region of the N-polar GaN HEMTs partially counteracts the electric field provided by the gate. It pushes the conduction band to the Fermi energy level (Figure 9), thus augmenting the 2DEG concentration [53]. This provides an intrinsic advantage wherein the Ga-polar devices cannot be duplicated, and demonstrates that only the N-polar GaN HEMTs are appropriate for the deep recess.

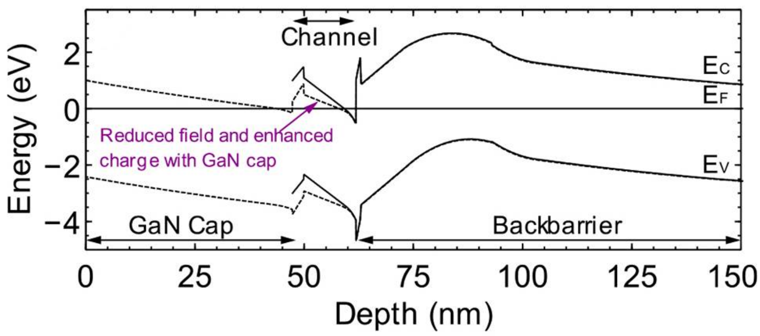

Figure 9. Energy band diagram comparing the N-polar GaN HEMT with and without a GaN cap. Reprinted with permission from Ref. [53]. Copyright 2018 by IEEE.

4.2. Research Advances

In 2011, Kolluri et al. [54] first designed and fabricated an N-polar GaN HEMT with a thick unintentionally doped (UID) GaN cap, i.e., NPDR MIS-HEMT, and found that a 120 nm UID GaN cap was sufficient to remove any RF dispersion in the device. Since the last decade, extensive efforts have been devoted to NPDR structures to eliminate RF dispersion in solid-state power devices.

Wienecke et al. [55] from UCSB broadened the operating frequency to W-band (80-100 GHz) by fabricating NPDR MIS-HEMT on a sapphire substrate in 2016, with a 75 nm gate length and T-shaped gate. After implementing a T-gate design, weakened parasitic capacitance enhances device RF performance (both f_T and f_{max}) to some extent [56].

The controlling dispersion ability is assessed using DC and 200 ns pulsed I–V tests. Figure 10a supports that the device's on-resistance (R_{on}) and I_{max} are 0.58 Ω and 1.5 A/mm, respectively, under the DC condition. Only a minimal current collapse occurs even in the pulsed measurement, demonstrating the deep recess structure's efficient dispersion administration in high-frequency devices. Thanks to this, the device achieves a 2.9 W/mm P_{out} with an associated PAE of 15.5% at a load of 94 GHz. The following year, this team significantly improved the NPDR structure design, i.e., gate-sidewall overlapping [49]; the 3D model is presented in Figure 11. A 30 nm overlap on the sidewall was introduced when depositing the gate metal (the gate was aligned to the bottom of the notch structure in the previous design). This design is believed to assist the drain-side gate in relieving the edge electric field while allowing the device to handle more significant voltage fluctuations (over 12 V) and raise this device's power density to double the previous density. As can be seen from the pulse diagram (Figure 10b), the wrapping of the metal gate around the sidewall does bring about amazing dispersion management (details of which will be discussed later), resulting in the absence of any current collapse and knee-out phenomenon. Furthermore, in the small-signal RF measurement (shown in Figure 10c), the f_T and f_{max} of this HEMT are extrapolated to be 113 and 323 GHz, respectively, when the V_{DS} and V_{GS} bias are set to 13 V and −1.75 V. N-polar GaN HEMTs passivated by MOCVD and PECVD SiN_x during the same period, on the contrary, tend to exhibit an undesirable dispersion behavior [57,58].

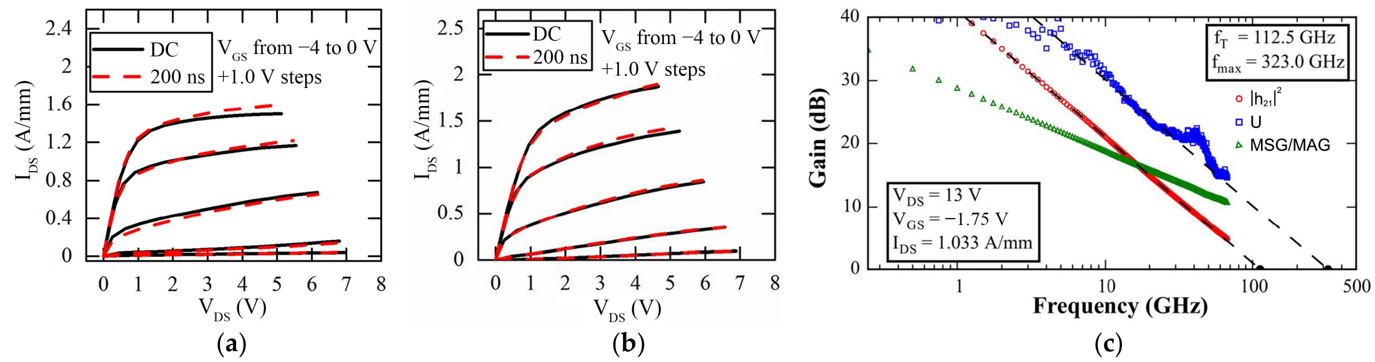

Figure 10. (**a**) DC and pulsed I_{DS}–V_{DS} measurements of the NPDR MIS-HEMT, fabricated by Wienecke et al. in 2016. Adapted with permission from Ref. [55]. Copyright 2016 by IEEE. (**b**) DC and pulsed I_{DS}–V_{DS} measurements and (**c**) small-signal RF performance of the NPDR MIS-HEMT with gate-sidewall overlapping, fabricated by Steven et al. in 2017. Adapted with permission from Ref. [49]. Copyright 2017 by IEEE.

The relationship between gate metal coverage of recessed regions and dispersion was further discussed by Wienecke [59]. In the case of a fully exposed sidewall, the dispersion aroused by the gap (refers to the space between the bottom of the gate metal and the groove, schematic diagram as shown in Figure 12) was first determined. Figure 13 exhibits the dispersion vs. the drain-side and source-side gap and the effect of different gate coverage on the output power and gate leakage current, respectively. When the gate metal covers the entire gate depression area (no gap and the sidewall is completely covered), the dispersion induced by those surface states on the sidewall is wholly removed. If the gap is minute (for example, 5 nm), the produced dispersion is negligible and can be acceptable. Once the gap approaches 50 nm or more, the RF dispersion will increase dramatically; hence, wide gaps over 50 nm are forbidden in NPDR structures. The gap discussed above relates to the drain side, whereas the source-side sidewall is completely covered, and a 50 nm field plate is used so that the experimental dispersion is mainly from the drain side. The same test procedure is applied to the source side, and a similar dispersion behavior is obtained. Results of gate coverage contribution to device performance suggest that the full metal coverage sample achieved the highest RF P_{out} of any transistor under the drain bias. However, it will cause a slight degradation in f_T/f_{max} due to the larger C_{gs} and C_{gd} [60]. The I_g drops rapidly with the increase of sidewall coverage, but the device with a 15 nm gap is even lower than that of the one with half of the sidewall covered; thus, the mechanism of gate metal deposition coverage on the gate leakage current should be further investigated. Weighing the device's frequency characteristics, breakdown and output power performance, Full Metal Coverage is considered the best trade-off solution. Most reports on NPDR structures currently use a self-alignment process to cover the entire gate depression region.

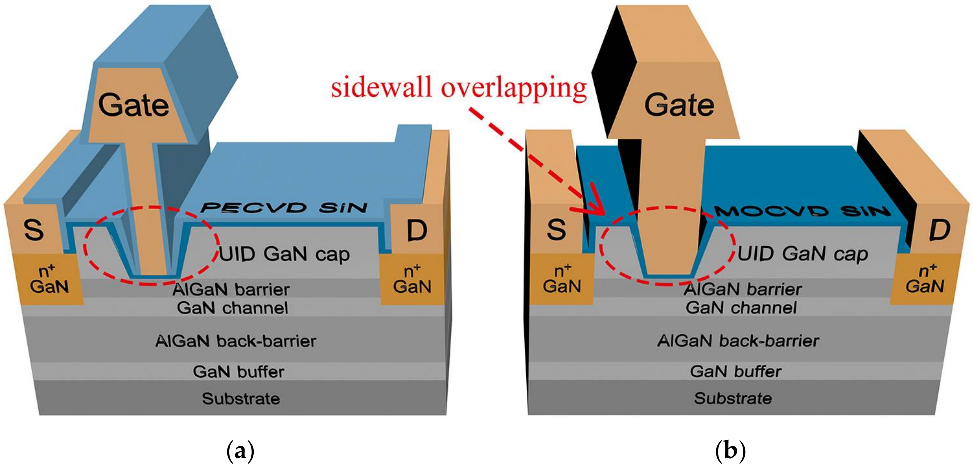

Figure 11. 3D model of NPDR MIS-HEMTs. (**a**) Without gate-sidewall overlapping; (**b**) with gate-sidewall overlapping.

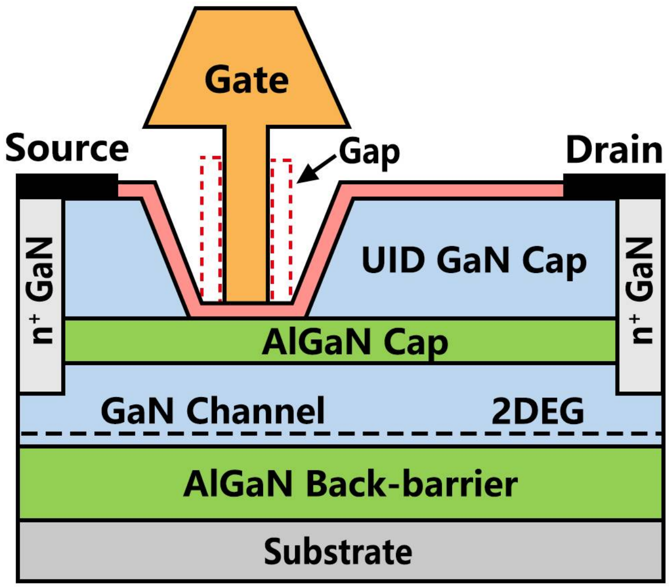

Figure 12. Schematic diagram of the gap between the gate metal and the GaN cap sidewalls.

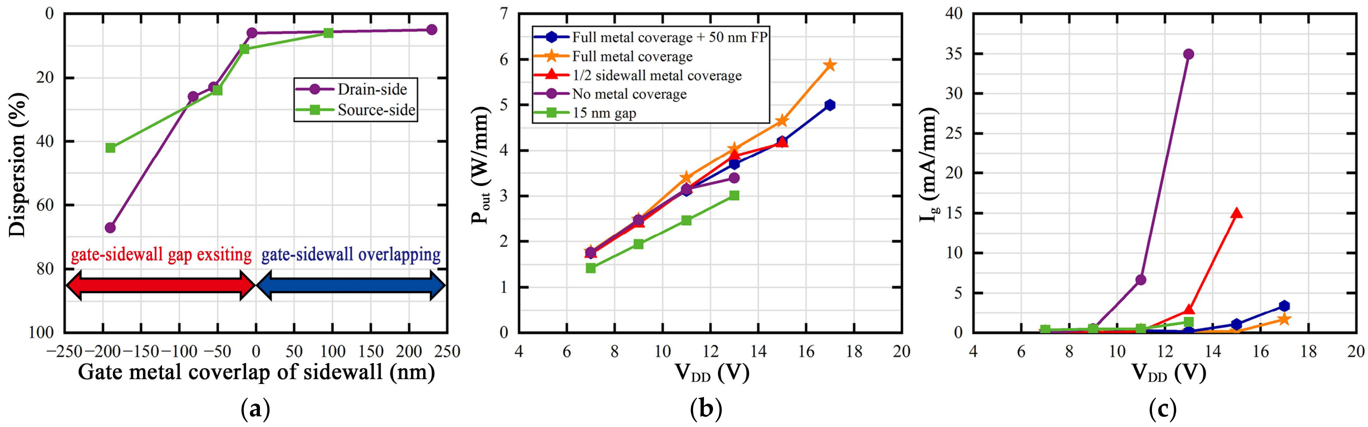

Figure 13. (**a**) Plots of the dispersion vs. source-side and drain-side gap. (**b**,**c**) The performance of output power and gate leakage current at different gate coverage. Reworked from Ref. [59].

The UID GaN cap thickness is also one of the crucial parameters in the NPDR structure. It is clear that the thicker the cap is, the further the channel is from the device surface, which minimizes the surface charge impact on the 2DEG and achieves superior dispersion control. 47.5 nm GaN cap thickness was found to be the most suited in earlier research until lately, this classic thickness has been replaced by 20 nm, primarily to reduce the fringing capacitance while still maintaining the high access region channel conductivity [61]. This action helps improve the device's gain and f_T/f_{max} combination but perhaps leads to incomplete dispersion control. While additional PECVD passivation can be used to compensate for the reduced ability to regulate dispersion and obtain the desired results.

UID GaN cap with PECVD SiN_x passivation to commonly suppress dispersion has been demonstrated and fabricated many times in N-polar GaN devices [55,61–63]. Utilization of the double-layer structure makes it possible to achieve excellent performance without the original thick cap, preventing parasitic channels caused by the strong polarization effect (PECVD SiN_x does not produce polarization). At the same time, gate misalignment inside the trench is inevitable during the gate deposition, and PECVD SiN_x is also effective in eliminating the remaining dispersion left by gate misalignment [55]. Regardless of the rationale, the additional SiN_x passivation does have beneficial effects on the breakdown and power performance of the device. Romanczyk found that depositing 40 nm PECVD SiN_x on the surface of a typical 47.5 nm UID GaN cap yielded higher output power at 10 GHz and allowed the HEMT to operate at higher $V_{DS,Q}$ (the SiN_x passivation increased $V_{T,access}$ so that the channel can withstand higher voltages without being depleted) [62]. Under pulsed I_{DS}–V_{DS} measurement (650 ns pulse with and 0.065% duty cycle), the I_D of the device drops only 8.5%, even with the stress as high as 23 V. Figure 14 compares the performance of this NPDR GaN HEMT with the superior Ga-polar monolithic microwave integrated circuit (MMIC) at W-band. When the load-pull measure is boosted to 94 GHz, a peak output power of 8.84 W/mm with 27% associated PAE (V_D = 23 V) made it the best-performing device among the N-polar GaN device family. A slight reduction in voltage (to 20 V) would show a peak PAE of 30.7%, also unprecedented in N-polar GaN devices to date. This result far exceeds the leading level in the W-band reported for Ga-polar devices (an MMIC reported by Niida et al. [64] achieving 3.6 W/mm P_{out} with a maximum PAE of 12.3%, and an AlN/GaN HEMT reported by Harrouche et al. [65] achieving 4 W/mm P_{out} with a PAE of 14.3% in 2019), proving the absolute dominance of NPDR structures in the millimeter-wave RF field.

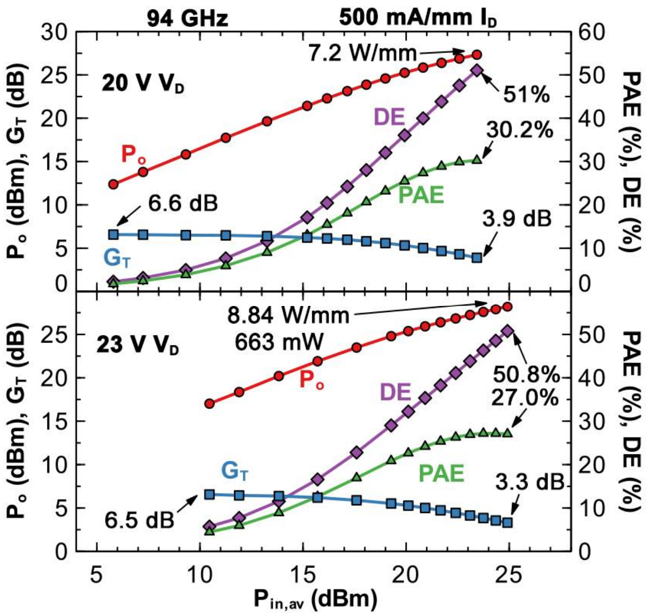

(**a**)

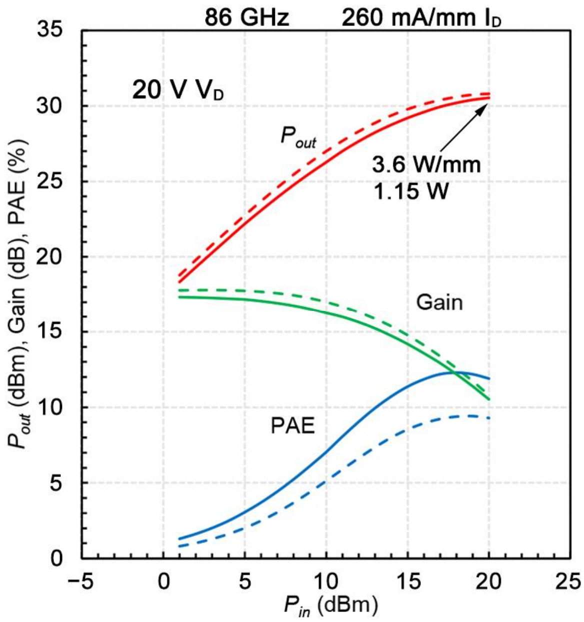

(**b**)

Figure 14. Power characteristics of devices in the W-band. (**a**) NPDR GaN HEMT reported by Romanczyk. Adapted with permission from Ref. [62]. Copyright 2020 by IEEE. (**b**) Advanced Ga-polar MMIC, the solid and dashed lines are the results in the actual measurement and simulation scenarios, respectively. Adapted with permission from Ref. [64]. Copyright 2016 by IEEE.

A thin double-cap layer structure, 2.6 nm of AlGaN deposited on top of 10 nm UID GaN as the cap layer, facilitates gain enhancement and suppresses parasitic channels [66]. At a 1 µs gate pulse width and an 800 ns drain pulse width, the test findings demonstrate that only around 10% dispersion ($V_{GS,Q} = -6$ V, $V_{DS,Q} = 0$ V) is observed. The gain enhancement due to the thin double-cap design facilitates the modulation effect of the gate on the 2DEG. It reduces the signal distortion of the device, enabling it to be more suitable for receivers that operate at low drain bias voltages.

More recently, Transphorm Inc. [67] has grown NPDR epitaxial stack on a 4-inch off-axis sapphire and a 4-inch off-axis C-face SiC substrates, respectively, and obtained excellent material quality characteristics for both, which demonstrates the feasibility of commercializing GaN NPDR MIS-HEMTS in the future. The STEM and typical AFM topography of the epitaxial stack are indicated in Figure 15. It can be seen in the STEM that the GaN buffer gradually filters out the linear dislocations starting from the nucleation layer to ensure the material quality in the upper HEMT region. In addition, there is a good hierarchical structure between the GaN and Al(Ga)N, with a low center-to-edge non-uniformity of about 0.3%. The low roughness average (R_a) of only 1.1 nm (on 100 mm sapphire) and 1.5 nm (on 100 mm SiC) reveals that the N-polar epitaxial layer has a smooth surface, implying success in the large-size N-polar GaN wafers' growth. Researchers at Transphorm Inc. also found a low average R_{sh} of 234.3 Ω/sq for the 2DEG channel (with a 2% non-uniformity) owing to the 2DEG with an electron density of about 1.44×10^{13} cm^{-2} and high electron mobility (is approximately 1850 cm^2/V·s). It is worth mentioning that these values are the average mobility measured in both the parallel and perpendicular directions to the miscut steps. Thus, higher mobility and lower R_{sh} may be obtained if the current moves precisely in the parallel direction (along the terrace direction) of the actual deep recess devices.

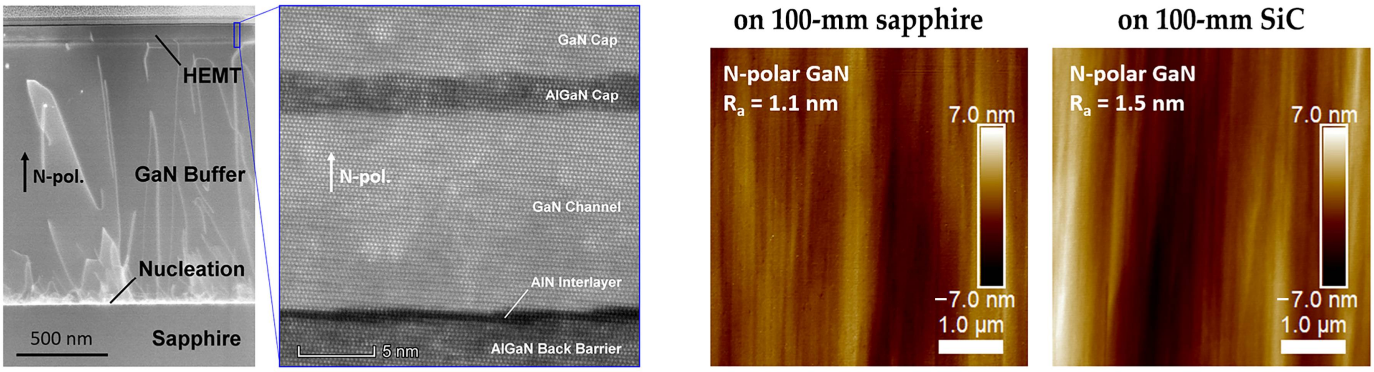

(**a**) (**b**)

Figure 15. (**a**) STEM cross-section of the N-polar GaN epitaxy and NPDR MIS-HEMT layers; (**b**) AFM topography image of N-polar GaN epitaxy on 100 mm sapphire and 100 mm miscut C-face SiC substrates. Adapted with permission from Ref. [67]. Copyright 2021 by IEEE.

The parameters and the performance of NPDR MIS-HEMTs operating in a range of frequencies are summarized in Table 2 for reference. The superior results imply that the NPDR structure is an efficient solution for suppressing surface dispersion of high-frequency devices, which may be commercially available and employed in the future RF industry, especially in the growing demand of the 5G market. However, it is necessary first to consider the poor heat dissipation caused by the current recovery. GaN-on-diamond may be a prospective option to address the thermal aggregation of NPDR GaN HEMTs in the future [68–70].

Table 2. Characterization of NPDR MIS-HEMTs applied to various wave bands, including epitaxial structures, output performances, and dispersion suppression.

Ref.	Band	Freq. (GHz)	Peak P_o			Peak PAE			Disp. (%)	Cap Thk. (nm)	SiN_x Thk. (nm)	Substrate
			V_D(V)	P_o (W/mm)	PAE (%)	V_D(V)	P_o (W/mm)	PAE (%)				
[55]			10	2.9	15.5	8	1.7	20		110	18	Sapphire
[60]			14	4.2		8	1.6	16.5		22	NO	Sapphire
[61]			16	5.5	20.6	12	3.7	25.9	<5	20	20	Sapphire
[71]			11	3.7		9	3.0	27.8	<5	47.5	NO	SiC
[72]	W	94	18	6.2	33.8	16	5.6	34.8		47.5	24	SiC
[49]			16	6.7	14.4	15	4.8	16.9	NO	47.5	NO	SiC
[73]			20	7.1	25.1	14	4.6	27.5		47.5	NO	SiC
[53]			20	7.9	26.9	16	5.3	28.8	<10	47.5	NO	SiC
[62]			23	8.8	27	20	7.2	30.2	8.5	47.5	40	SiC
[74]		87				8	2.5	34.2	NO	47.5	NO	SiC
[66]									10	12.6	20	SiC
[53]	Ka	30	20	8.1	52.5	14	5.6	55.9	<10	47.5	NO	SiC
[63]			26	10.3	47.4					47.5	40	SiC
[53]	X	10	20	7.8	54.9	14	5.1	58.1	<10	47.5	NO	SiC
[54]	C	4	24	5.5	74				NO	120	NO	Sapphire

5. Conclusions

GaN-based HEMTs have shown great performance in the microwave RF field. Nevertheless, the inherent high-density surface states of GaN and the inevitable defects during fabricating are potential sources of surface traps. In the switching transition of the device, the behaviors of trapping and delayed releasing electrons by the surface states are the leading causes of RF surface dispersion and pose a significant challenge to HEMTs to maintain high output power and stability. Accordingly, how to suppress RF dispersion in GaN devices is an interesting research problem.

Surface treatment, passivation, field plate, GaN cap layer, and Si surface doping are demonstrated to effectively suppress RF dispersion and are widely used in the industry.

While these methods provide varying degrees of dispersion suppression, as higher frequencies are explored, the exacerbated surface trapping effect or excessive parasitic capacitance makes these techniques progressively less effective.

N-polar GaN has many special advantages in high-frequency applications due to the opposite polarity, especially allowing the growth of a thick GaN channel (or thick UID GaN cap on the access region), providing an alternative way to minimize the dispersion caused by surface trapping at high frequencies. The utilization of a thick GaN layer keeps the surface far from the 2DEG channel to control the surface states and minimize the impact of surface charging on device operation. The isolation between the channel and the surface enables the NPDR structure to be considered the most promising approach for solving RF dispersion in GaN-based high-frequency power devices. In the past decade, the structural design of NPDR has been continuously improved, such as self-alignment for full coverage of the depression region with gate metal, simultaneous use of deep recess structure and SiN_x passivation, and a double-layer structure for the receiver side. From the results, NPDR is expected to significantly contribute to the elimination of RF dispersion in high-frequency GaN HEMTs, restore their stability and inherent high power density, and is likely to be used in commercial 5G millimeter-wave RF devices in the future. However, the high price of SiC substrates, the high-quality requirements for N-polar GaN epitaxy, and heat dissipation are the primary impediments to large-scale industrial fabrication. Therefore, if more substantial progress can be achieved in addressing these obstacles, the application prospects of high-frequency GaN HEMTs will extend further.

Author Contributions: Conceptualization, P.Z. and X.G.; investigation, X.N. and Q.F.; resources, X.N. and Q.F; data curation, P.Z. and X.G.; visualization, P.Z.; writing—original draft preparation, P.Z.; writing—review and editing, X.G.; funding acquisition, X.G. All authors have read and agreed to the published version of the manuscript.

Funding: This research was funded by the National Nature Science Foundation of China, grant number 62074033.

Data Availability Statement: Not applicable.

Acknowledgments: The authors would like to thank Maxwell QH from Dulwich College Suzhou for his contribution to the English language and style in this work.

Conflicts of Interest: The authors declare no conflict of interest.

References

1. Fujita, S. Wide-bandgap semiconductor materials: For their full bloom. *Jpn. J. Appl. Phys.* **2015**, *54*, 030101. [CrossRef]
2. Roccaforte, F.; Fiorenza, P.; Greco, G.; Lo Nigro, R.; Giannazzo, F.; Iucolano, F.; Saggio, M. Emerging trends in wide band gap semiconductors (SiC and GaN) technology for power devices. *Microelectron. Eng.* **2018**, *187–188*, 66–77. [CrossRef]
3. Dubey, S.K.; Mishra, M.; Islam, A. Characterization of ALGAN / GAN based HEMT for low noise and high frequency application. *Int. J. Numer. Model.* **2022**, *35*, e2932. [CrossRef]
4. Chen, S.; Witkowski, L.; Gu, X. (Invited) Important Recent Advancement of GaN Technology and MMICs for W-Band Applications. *ECS Trans.* **2017**, *80*, 945–952. [CrossRef]
5. Ye, R.; Cai, X.; Du, C.; Liu, H.; Zhang, Y.; Duan, X.; Zhu, J. An Overview on Analyses and Suppression Methods of Trapping Effects in AlGaN/GaN HEMTs. *IEEE Access* **2022**, *10*, 21759–21773. [CrossRef]
6. Rongming, C.; Likun, S.; Fichtenbaum, N.; Zhen, C.; Keller, S.; DenBaars, S.P.; Mishra, U.K. Correlation Between DC–RF Dispersion and Gate Leakage in Deeply Recessed GaN/AlGaN/GaN HEMTs. *IEEE Electron Device Lett.* **2008**, *29*, 303–305. [CrossRef]
7. Rawal, D.S.; Amit; Sharma, S.; Kapoor, S.; Laishram, R.; Vinayak, S. Current collapse scaling in GaN/AlGaN/SiC high electron mobility transistors. *Solid State Electron. Lett.* **2019**, *1*, 30–37. [CrossRef]
8. Shuxun, L.; Maoju, W.; Bing, X.; Wen, C.P.; Min, Y.; Jinyan, W.; Yilong, H.; Wengang, W.; Sen, H.; Chen, K.J. Bo Shen Reduction of Current Collapse in GaN High-Electron Mobility Transistors Using a Repeated Ozone Oxidation and Wet Surface Treatment. *IEEE Electron Device Lett.* **2015**, *36*, 757–759. [CrossRef]
9. Madan, J.; Pandey, R.; Arora, H.; Chaujar, R. Analysis of Varied Dielectrics as Surface Passivation on AlGaN/GaN HEMT for Analog Applications. In Proceedings of the 2018 6th Edition of International Conference on Wireless Networks & Embedded Systems (WECON), Rajpura, India, 16–17 November 2018; pp. 15–18.

10. Hasan, M.T.; Asano, T.; Tokuda, H.; Kuzuhara, M. Current Collapse Suppression by Gate Field-Plate in AlGaN/GaN HEMTs. *IEEE Electron Device Lett.* **2013**, *34*, 1379–1381. [CrossRef]
11. Sarkar, S.; Khade, R.P.; DasGupta, A.; DasGupta, N. Effect of GaN cap layer on the performance of AlInN/GaN-based HEMTs. *Microelectron. Eng.* **2022**, *258*, 111756. [CrossRef]
12. Song, L.; Fu, K.; Zhang, Z.; Sun, S.; Li, W.; Yu, G.; Hao, R.; Fan, Y.; Shi, W.; Cai, Y.; et al. Interface Si donor control to improve dynamic performance of AlGaN/GaN MIS-HEMTs. *AIP Adv.* **2017**, *7*, 125023. [CrossRef]
13. Longobardi, G.; Udrea, F.; Sque, S.; Hurkx, G.A.M.; Croon, J.; Napoli, E.; Sonsky, J. Impact of Donor Traps on the 2DEG and Electrical Behavior of AlGaN/GaN MISFETs. *IEEE Electron Device Lett.* **2014**, *35*, 27–29. [CrossRef]
14. Miczek, M.; Mizue, C.; Hashizume, T.; Adamowicz, B. Effects of interface states and temperature on the C-V behavior of metal/insulator/AlGaN/GaN heterostructure capacitors. *J. Appl. Phys.* **2008**, *103*, 104510. [CrossRef]
15. Green, B.M.; Chu, K.K.; Chumbes, E.M.; Smart, J.A.; Shealy, J.R.; Eastman, L.F. The effect of surface passivation on the microwave characteristics of undoped AlGaN/GaN HEMTs. *IEEE Electron Device Lett.* **2000**, *21*, 268–270. [CrossRef]
16. Jogai, B. Influence of surface states on the two-dimensional electron gas in AlGaN/GaN heterojunction field-effect transistors. *J. Appl. Phys.* **2003**, *93*, 1631–1635. [CrossRef]
17. Ibbetson, J.P.; Fini, P.T.; Ness, K.D.; DenBaars, S.P.; Speck, J.S.; Mishra, U.K. Polarization effects, surface states, and the source of electrons in AlGaN/GaN heterostructure field effect transistors. *Appl. Phys. Lett.* **2000**, *77*, 250–252. [CrossRef]
18. Vetury, R.; Zhang, N.Q.; Keller, S.; Mishra, U.K. The impact of surface states on the DC and RF characteristics of AlGaN/GaN HFETs. *IEEE Trans. Electron Devices* **2001**, *48*, 560–566. [CrossRef]
19. Hwang, I.; Kim, J.; Chong, S.; Choi, H.-S.; Hwang, S.-K.; Oh, J.; Shin, J.K.; Chung, U.-I. Impact of Channel Hot Electrons on Current Collapse in AlGaN/GaN HEMTs. *IEEE Electron Device Lett.* **2013**, *34*, 1494–1496. [CrossRef]
20. Meneghesso, G.; Verzellesi, G.; Pierobon, R.; Rampazzo, F.; Chini, A.; Mishra, U.K.; Canali, C.; Zanoni, E. Surface-Related Drain Current Dispersion Effects in AlGaN–GaN HEMTs. *IEEE Trans. Electron Devices* **2004**, *51*, 1554–1561. [CrossRef]
21. Patanvariya, D.G.; Kumar, S.; Giri, L.I. Influence of Current Collapse in AlGaN/GaN High Electron Mobility Transistors. In Proceedings of the 2019 10th International Conference on Computing, Communication and Networking Technologies (ICCCNT), Kanpur, India, 6–8 July 2019; pp. 1–5.
22. Huang, H.; Liang, Y.C.; Samudra, G.S.; Chang, T.-F.; Huang, C.-F. Effects of Gate Field Plates on the Surface State Related Current Collapse in AlGaN/GaN HEMTs. *IEEE Trans. Power Electron.* **2014**, *29*, 2164–2173. [CrossRef]
23. Tingting, Y.; Xinyu, L.; Yingkui, Z.; Chengzhan, L.; Ke, W.; Guoguo, L. Impact of UV/ozone surface treatment on AlGaN/GaN HEMTs. *J. Semicond.* **2009**, *30*, 124001. [CrossRef]
24. King, S.W.; Barnak, J.P.; Bremser, M.D.; Tracy, K.M.; Ronning, C.; Davis, R.F.; Nemanich, R.J. Cleaning of AlN and GaN surfaces. *J. Appl. Phys.* **1998**, *84*, 5248–5260. [CrossRef]
25. Diale, M.; Auret, F.D.; van der Berg, N.G.; Odendaal, R.Q.; Roos, W.D. Analysis of GaN cleaning procedures. *Appl. Surf. Sci.* **2005**, *246*, 279–289. [CrossRef]
26. Kim, J.H.; Choi, H.G.; Ha, M.-W.; Song, H.J.; Roh, C.H.; Lee, J.H.; Park, J.H.; Hahn, C.-K. Effects of Nitride-Based Plasma Pretreatment Prior to SiN_x Passivation in AlGaN/GaN High-Electron-Mobility Transistors on Silicon Substrates. *Jpn. J. Appl. Phys.* **2010**, *49*, 04DF05.
27. Romero, M.F.; Jimenez, A.; Miguel-Sanchez, J.; Brana, A.F.; Gonzalez-Posada, F.; Cuerdo, R.; Calle, F.; Munoz, E. Effects of N-2 plasma pretreatment on the SiN passivation of AlGaN/GaN HEMT. *IEEE Electron Device Lett.* **2008**, *29*, 209–211. [CrossRef]
28. Shih-Chien, L.; Bo-Yuan, C.; Yueh-Chin, L.; Ting-En, H.; Huan-Chung, W.; Chang, E.Y. GaN MIS-HEMTs With Nitrogen Passivation for Power Device Applications. *IEEE Electron Device Lett.* **2014**, *35*, 1001–1003. [CrossRef]
29. Mi, M.; Lu, Y.; Hao, Y.; Ma, X.; Yang, L.; Hou, B.; Zhang, M. Improved f_{max} and breakdown voltage in AlGaN/GaN HEMT with plasma treatment. In Proceedings of the 2018 1st Workshop on Wide Bandgap Power Devices and Applications in Asia (WiPDA Asia), Xi'an, China, 16–18 May 2018; pp. 208–211.
30. Machuca, F.; Liu, Z.; Sun, Y.; Pianetta, P.; Spicer, W.E.; Pease, R.F.W. Simple method for cleaning gallium nitride (0001). *J. Vac. Sci. Technol. A Vac. Surf. Film.* **2002**, *20*, 1784–1786. [CrossRef]
31. Geng, K.; Chen, D.; Zhou, Q.; Wang, H. AlGaN/GaN MIS-HEMT with PECVD SiNx, SiON, SiO2 as Gate Dielectric and Passivation Layer. *Electronics* **2018**, *7*, 416. [CrossRef]
32. Grabow, L.C.; Uhlrich, J.J.; Kuech, T.F.; Mavrikakis, M. Effectiveness of in situ NH3 annealing treatments for the removal of oxygen from GaN surfaces. *Surf. Sci.* **2009**, *603*, 387–399. [CrossRef]
33. Cheng, K.-Y.; Wu, S.-C.; Yu, C.-J.; Wang, T.-W.; Liao, J.-H.; Wu, M.-C. Comparative study on performance of AlGaN/GaN MS-HEMTs with SiNx, SiOx, and SiNO surface passivation. *Solid-State Electron.* **2020**, *170*, 107824. [CrossRef]
34. Huang, T.; Malmros, A.; Bergsten, J.; Gustafsson, S.; Axelsson, O.; Thorsell, M.; Rorsman, N. Suppression of Dispersive Effects in AlGaN/GaN High-Electron-Mobility Transistors Using Bilayer SiN_x Grown by Low Pressure Chemical Vapor Deposition. *IEEE Electron Device Lett.* **2015**, *36*, 537–539. [CrossRef]
35. Zhao, S.-X.; Liu, X.-Y.; Zhang, L.-Q.; Huang, H.-F.; Shi, J.-S.; Wang, P.-F. Impacts of Thermal Atomic Layer-Deposited AlN Passivation Layer on GaN-on-Si High Electron Mobility Transistors. *Nanoscale Res. Lett.* **2016**, *11*, 137. [CrossRef] [PubMed]
36. Huang, S.; Jiang, Q.; Yang, S.; Zhou, C.; Chen, K.J. Effective Passivation of AlGaN/GaN HEMTs by ALD-Grown AlN Thin Film. *IEEE Electron Device Lett.* **2012**, *33*, 516–518. [CrossRef]

37. Liu, S.C.; Wong, Y.-Y.; Lin, Y.-C.; Chang, E.Y. Low Current Collapse and Low Leakage GaN MIS-HEMT Using AlN/SiN as Gate Dielectric and Passivation Layer. *ECS Trans.* **2014**, *61*, 211–214. [CrossRef]
38. Huang, T.; Bergsten, J.; Thorsell, M.; Rorsman, N. Small- and Large-Signal Analyses of Different Low-Pressure-Chemical-Vapor-Deposition SiN_x Passivations for Microwave GaN HEMTs. *IEEE Trans. Electron Devices* **2018**, *65*, 908–914. [CrossRef]
39. Godfrey, D.; Nirmal, D.; Arivazhagan, L.; Godwinraj, D.; Mohan Kumar, N.; Chen, Y.; Yeh, W. Current collapse degradation in GaN High Electron Mobility Transistor by virtual gate. *Microelectron. J.* **2021**, *118*, 105293. [CrossRef]
40. Arulkumaran, S.; Egawa, T.; Ishikawa, H. Studies on the Influences of *i* -GaN, *n* -GaN, *p* -GaN and InGaN Cap Layers in AlGaN/GaN High-Electron-Mobility Transistors. *Jpn. J. Appl. Phys.* **2005**, *44*, 2953–2960. [CrossRef]
41. Kordoš, P.; Bernát, J.; Marso, M. Impact of layer structure on performance of unpassivated AlGaN/GaN HEMT. *Microelectron. J.* **2005**, *36*, 438–441. [CrossRef]
42. Mitrofanov, O.; Manfra, M.; Weimann, N. Impact of Si doping on radio frequency dispersion in unpassivated GaN/AlGaN/GaN high-electron-mobility transistors grown by plasma-assisted molecular-beam epitaxy. *Appl. Phys. Lett.* **2003**, *82*, 4361–4363. [CrossRef]
43. Gambin, V.; Gu, X.; Heying, B. AIN buffer N-polar GaN HEMT Profile. Patent US8710511B2, 4 April 2014.
44. Gambin, V.; GU, X. Ingan channel n-polar gan hemt Profile. Patent WO2014031229A1, 27 February 2014.
45. Wong, M.H.; Keller, S.; Nidhi, S.D.; Denninghoff, D.J.; Kolluri, S.; Brown, D.F.; Lu, J.; Fichtenbaum, N.A.; Ahmadi, E.; Singisetti, U.; et al. N-polar GaN epitaxy and high electron mobility transistors. *Semicond. Sci. Technol.* **2013**, *28*, 074009. [CrossRef]
46. Nakajima, A.; Fujii, K.; Horio, K. Numerical Analysis of Buffer-Trap Effects on Gate Lag in AlGaN/GaN High Electron Mobility Transistors. *Jpn. J. Appl. Phys.* **2011**, *50*, 104303. [CrossRef]
47. Smorchkova, I.; Grundbacher, R.; Gambin, V.; Gu, X.; Lewis, G.; Oshita, F.; Namba, C.; Liu, P.; Poust, S.; Nam, P.; et al. N-Face GaN HEMT Technology for Next-Generation Mixed-Signal Electronics. In Proceedings of the 37th Annual GOMACTech Conference, Las Vegas, NV, USA, 19–22 March 2012.
48. Gu, X.; Xie, J.; Lee, C. Process of fabricating high efficiency, high linearity N-polar gallium-nitride (GaN) Transistors. Patent US10749009B1, 18 August 2020.
49. Steven, W.; Romanczyk, B.; Guidry, M.; Li, H.; Ahmadi, E.; Hestroffer, K.; Zheng, X.; Keller, S.; Mishra, U.K. N-Polar GaN Cap MISHEMT With Record Power Density Exceeding 6.5 W/mm at 94 GHz. *IEEE Electron Device Lett.* **2017**, *38*, 359–362.
50. Shen, L.; Coffie, R.; Buttari, D.; Heikman, S.; Chakraborty, A.; Chini, A.; Keller, S.; DenBaars, S.P.; Mishra, U.K. High-Power Polarization-Engineered GaN/AlGaN/GaN HEMTs Without Surface Passivation. *IEEE Electron Device Lett.* **2004**, *25*, 7–9. [CrossRef]
51. Shen, L.; Palacios, T.; Poblenz, C.; Corrion, A.; Chakraborty, A.; Fichtenbaum, N.; Keller, S.; Denbaars, S.P.; Speck, J.S.; Mishra, U.K. Unpassivated high power deeply recessed GaN HEMTs with fluorine-plasma surface treatment. *IEEE Electron Device Lett.* **2006**, *27*, 214–216. [CrossRef]
52. Shen, L.; Pei, Y.; McCarthy, L.; Poblenz, C.; Corrion, A.; Fichtenbaum, N.; Keller, S.; Denbaars, S.P.; Speck, J.S.; Mishra, U.K. Deep-recessed GaN HEMTs using selective etch technology exhibiting high microwave performance without surface passivation. In Proceedings of the 2007 IEEE/MTT-S International Microwave Symposium, Honolulu, HI, USA, 3–8 June 2007; pp. 623–626.
53. Romanczyk, B.; Wienecke, S.; Guidry, M.; Li, H.; Ahmadi, E.; Zheng, X.; Keller, S.; Mishra, U.K. Demonstration of Constant 8 W/mm Power Density at 10, 30, and 94 GHz in State-of-the-Art Millimeter-Wave N-Polar GaN MISHEMTs. *IEEE Trans. Electron Devices* **2018**, *65*, 45–50. [CrossRef]
54. Kolluri, S.; Brown, D.F.; Wong, M.H.; Dasgupta, S.; Keller, S.; DenBaars, S.P.; Mishra, U.K. RF Performance of Deep-Recessed N-Polar GaN MIS-HEMTs Using a Selective Etch Technology Without Ex Situ Surface Passivation. *IEEE Electron Device Lett.* **2011**, *32*, 134–136. [CrossRef]
55. Wienecke, S.; Romanczyk, B.; Guidry, M.; Li, H.; Zheng, X.; Ahmadi, E.; Hestroffer, K.; Megalini, L.; Keller, S.; Mishra, U.K. N-Polar Deep Recess MISHEMTs with Record 2.9 W/mm at 94 GHz. *IEEE Electron Device Lett.* **2016**, *37*, 713–716. [CrossRef]
56. Mohapatra, M.; De, T.; Panda, A.K. Performance analysis of AlGaN/GaN based HEMT for different gate structure (Normal gate and T-shaped gate). In Proceedings of the 2017 Devices for Integrated Circuit (DevIC), Kalyani, India, 23–24 March 2017; pp. 144–148.
57. Zheng, X.; Guidry, M.; Li, H.; Romanczyk, B.; Ahmadi, E.; Hestroffer, K.; Wienecke, S.; Keller, S.; Mishra, U.K. N-polar GaN MIS-HEMTs on sapphire with a proposed figure of merit fmax·VDS, Q of 9.5 THz.V. In Proceedings of the 2017 75th Annual Device Research Conference (DRC), South Bend, IN, USA, 25–28 June 2017; pp. 1–2.
58. Zheng, X.; Li, H.; Ahmadi, E.; Hestroffer, K.; Guidry, M.; Romanczyk, B.; Wienecke, S.; Keller, S.; Mishra, U.K. High frequency N-polar GaN planar MIS-HEMTs on sapphire with high breakdown and low dispersion. In Proceedings of the 2016 Lester Eastman Conference (LEC), Bethlehem, PA, USA, 2–4 August 2016; pp. 42–45.
59. Wienecke, S.M. N-Polar Deep Recess MISHEMTs for mm-Wave Applications. Ph.D. Thesis, University of California-Santa Barbara, Los Angeles, CA, USA, 2018.
60. Romanczyk, B.; Wienecke, S.; Guidry, M.; Li, H.; Hestroffer, K.; Ahmadi, E.; Zheng, X.; Keller, S.; Mishra, U.K. mm-Wave N-polar GaN MISHEMT with a self-aligned recessed gate exhibiting record 4.2 W/mm at 94 GHz on Sapphire. In Proceedings of the 2016 74th Annual Device Research Conference (DRC), Newark, DE, USA, 19–22 June 2016; pp. 1–2.
61. Romanczyk, B.; Li, W.; Guidry, M.; Hatui, N.; Krishna, A.; Wurm, C.; Keller, S.; Mishra, U.K. N-Polar GaN-on-Sapphire Deep Recess HEMTs With High W-Band Power Density. *IEEE Electron Device Lett.* **2020**, *41*, 1633–1636. [CrossRef]

62. Romanczyk, B.; Zheng, X.; Guidry, M.; Li, H.; Hatui, N.; Wurm, C.; Krishna, A.; Ahmadi, E.; Keller, S.; Mishra, U.K. W-Band Power Performance of SiN-Passivated N-Polar GaN Deep Recess HEMTs. *IEEE Electron Device Lett.* **2020**, *41*, 349–352. [CrossRef]
63. Romanczyk, B.; Guidry, M.; Zheng, X.; Shrestha, P.; Li, H.; Ahmadi, E.; Keller, S.; Mishra, U.K. Evaluation of linearity at 30 GHz for N-polar GaN deep recess transistors with 10.3 W/mm of output power and 47.4% PAE. *Appl. Phys. Lett.* **2021**, *119*, 072105. [CrossRef]
64. Niida, Y.; Kamada, Y.; Ohki, T.; Ozaki, S.; Makiyama, K.; Minoura, Y.; Okamoto, N.; Sato, M.; Joshin, K.; Watanabe, K. 3.6 W/mm high power density W-band InAlGaN/GaN HEMT MMIC power amplifier. In Proceedings of the 2016 IEEE Topical Conference on Power Amplifiers for Wireless and Radio Applications (PAWR), Austin, TX, USA, 24–27 January 2016; pp. 24–26.
65. Harrouche, K.; Kabouche, R.; Okada, E.; Medjdoub, F. High Performance and Highly Robust AlN/GaN HEMTs for Millimeter-Wave Operation. *IEEE J. Electron Devices Soc.* **2019**, *7*, 1145–1150. [CrossRef]
66. Shrestha, P.; Guidry, M.; Romanczyk, B.; Hatui, N.; Wurm, C.; Krishna, A.; Pasayat, S.S.; Karnaty, R.R.; Keller, S.; Buckwalter, J.F.; et al. High Linearity and High Gain Performance of N-Polar GaN MIS-HEMT at 30 GHz. *IEEE Electron Device Lett.* **2020**, *41*, 681–684. [CrossRef]
67. Bisi, D.; Romanczyk, B.; Liu, X.; Gupta, G.; Brown-Heft, T.; Birkhahn, R.; Lal, R.; Neufeld, C.J.; Keller, S.; Parikh, P.; et al. Commercially Available N-polar GaN HEMT Epitaxy for RF Applications. In Proceedings of the 2021 IEEE 8th Workshop on Wide Bandgap Power Devices and Applications (WiPDA), Redondo Beach, CA, USA, 7–9 November 2021; pp. 250–254.
68. Gu, X.; Lee, C.; Xie, J.; Beam, E.; Becker, M.; Grotjohn, T.; Anaya, J.; Kuball, M. *GaN-on-Diamond with Ultra-Low Thermal Barrier Resistance*; Qorvo Inc.: Richardson, TX, USA, 2016.
69. Zhou, Y.; Anaya, J.; Pomeroy, J.; Sun, H.; Gu, X.; Xie, A.; Beam, E.; Becker, M.; Grotjohn, T.A.; Lee, C.; et al. Barrier-Layer Optimization for Enhanced GaN-on-Diamond Device Cooling. *ACS Appl. Mater. Interfaces* **2017**, *9*, 34416–34422. [CrossRef] [PubMed]
70. Yates, L.; Anderson, J.; Gu, X.; Lee, C.; Bai, T.; Mecklenburg, M.; Aoki, T.; Goorsky, M.S.; Kuball, M.; Piner, E.L.; et al. Low Thermal Boundary Resistance Interfaces for GaN-on-Diamond Devices. *ACS Appl. Mater. Interfaces* **2018**, *10*, 24302–24309. [CrossRef] [PubMed]
71. Romanczyk, B.; Guidry, M.; Wienecke, S.; Li, H.; Ahmadi, E.; Zheng, X.; Keller, S.; Mishra, U.K. W-band N-polar GaN MISHEMTs with high power and record 27.8% efficiency at 94 GHz. In Proceedings of the 2016 IEEE International Electron Devices Meeting (IEDM), San Francisco, CA, USA, 3–7 December 2016; pp. 3.5.1–3.5.4.
72. Liu, W.; Romanczyk, B.; Guidry, M.; Hatui, N.; Wurm, C.; Li, W.; Shrestha, P.; Zheng, X.; Keller, S.; Mishra, U.K. 6.2 W/Mm and Record 33.8% PAE at 94 GHz From N-Polar GaN Deep Recess MIS-HEMTs With ALD Ru Gates. *IEEE Microw. Wirel. Compon. Lett.* **2021**, *31*, 748–751. [CrossRef]
73. Romanczyk, B.; Guidry, M.; Zheng, X.; Li, H.; Ahmadi, E.; Keller, S.; Mishra, U.K. Bias-Dependent Electron Velocity Extracted From N-Polar GaN Deep Recess HEMTs. *IEEE Trans. Electron Devices* **2020**, *67*, 1542–1546. [CrossRef]
74. Romanczyk, B.; Guidry, M.; Wienecke, S.; Li, H.; Ahmadi, E.; Zheng, X.; Keller, S.; Mishra, U.K. Record 34.2% efficient mm-wave N-polar AlGaN/GaN MISHEMT at 87 GHz. *Electron. Lett.* **2016**, *52*, 1813–1814. [CrossRef]